Microscopic analysis of single-fiber push-out tests on ceramic matrix composites performed with Berkovich and flat-end indenter and evaluation of interfacial fracture toughness

W.M. Mueller, Judith Moosburger-Will, Markus G. R. Sause, Siegfried R. Horn

Angaben zur Veröffentlichung / Publication details:

Mueller, W.M., Judith Moosburger-Will, Markus G. R. Sause, and Siegfried R. Horn. 2013. "Microscopic analysis of single-fiber push-out tests on ceramic matrix composites performed with Berkovich and flat-end indenter and evaluation of interfacial fracture toughness." *Journal of the European Ceramic Society* 33 (2): 441–51. https://doi.org/10.1016/j.jeurceramsoc.2012.09.009.

Microscopic analysis of single-fiber push-out tests on ceramic matrix composites performed with Berkovich and flat-end indenter and evaluation of interfacial fracture toughness

W.M. Mueller*, J. Moosburger-Will, M.G.R. Sause, S. Horn

University of Augsburg, Institute for Physics, Experimental Physics II, D-86135 Augsburg, Germany

Abstract

Single-fiber push-out tests performed with a Berkovich and a flat-end indenter tip were conducted on the same SiC/PyC/SiC ceramic matrix composite sample for comparison. Push-out measurements were stopped at different stages during the experiment for a detailed microscopic analysis of the front and back side of the sample, to investigate the progression of failure during push-out process. The microscopic analyses reveal differences from the established interpretations which are crucial for quantitative evaluation of interface properties. Based on the microscopic findings, a modified loading schedule comprising unloading–reloading cycles is proposed, which provides access to the dissipative and non-dissipative energy contributions during push-out test. A new energy-based approach is presented which allows for the determination of the interfacial fracture toughness, without assumptions regarding the stress distribution along the interface to be made. Presuming stable crack growth along the complete debonding length, the interfacial fracture toughness of the sample investigated amounts to $44 \pm 9\ \mathrm{J/m^2}$.

Keywords: Single-fiber push-out test; Composites; Interfaces; Mechanical properties; SiC

1. Introduction

Ceramic matrix composites (CMC) are considered to be attractive candidates for long term applications in harsh environments, comprising high temperatures, high stress levels and corrosive atmospheres, e.g., in future transportation and energetic systems. It is well recognized that the mechanical performance of fiber-reinforced ceramic matrix composites under load, especially the intended damage-tolerant fracture behavior, is strongly related to the fiber–matrix interfacial properties.[1,2] In silicon carbide fiber-reinforced silicon carbide matrix composites (SiC/SiC), single- or multi-layered fiber coatings (e.g., pyrolytic carbon (PyC) coatings) are applied to enable micro crack deflection and fiber–matrix debonding.

The single-fiber push-out test, introduced by Marshall[3] in 1984, is a powerful testing method to evaluate the interfacial properties of CMC samples. For this purpose, a thin and plane-parallel composite sample (typically below 100 μm in thickness) is mounted on a sample holder with a groove located below the fibers to be tested. During single-fiber push-out test, an individual fiber is loaded by a diamond indenter tip with an increasing load resulting in fiber–matrix debonding and fiber push-out. Both pyramidal indenter tips[4–7] and flat-end indenter tips[8,9] are used for push-out tests. The interfacial parameters are extracted from load–displacement curves recorded during the experiment. There are different methods for evaluation described in literature, among these the evaluation of interfacial shear strength τ_{is} which is based on a simple force balance at the moment of push-out

$$\tau_{\mathrm{is}} = \frac{P}{2\pi r_{\mathrm{f}} L} \tag{1}$$

where P is the load at push-out, r_{f} is the fiber radius and L the fiber length.[3,4,10,11] Other evaluation methods depend on adjusting interfacial parameters, such as the stress for initial debonding, the radial stress at the interface, the residual axial stress in the fiber and the coefficient of friction, to fit the experimental curves according to the push-out models discussed in literature.[12–15,7,16,8]

* Corresponding author. Tel.: +49 821 598 3422; fax: +49 821 598 3411.

For an interpretation of the push-out test and evaluation of interfacial properties, a detailed understanding of the microscopic process taking place during the experiment is absolutely essential. Microscopic imagery of the push-out sample prior and subsequent to the test, as published in relevant literature, can not sufficiently clarify the progression of failure.

For that reason, a detailed microscopic analysis of the front and back side of a SiC/PyC/SiC composite sample is presented in this study, from measurements that were stopped at different stages during the push-out test. The microscopic analysis was executed on push-out tests performed with both a pyramidal indenter tip and a flat-end indenter tip. The use of a flat-end indenter tip increases the contact area between the indenter and the fiber and therefore reduces the indenter penetration. This leads to less fiber deformation and a reduction of radial Poisson's expansion compared to the pyramidal tip. Moreover, the smaller included angle of the flat-end tip allows a larger fiber displacement without the indenter touching the matrix. The experiments with both tips were performed on the same sample in order to enable a direct comparison of load–displacement curves and demonstrate the different values obtained for the interfacial shear strength τ_{is}.

Crack propagation at the interface is one of the dissipative processes during fiber–matrix debonding, contributing to a damage-tolerant fracture behavior. Therefore, the interfacial fracture toughness is a crucial quantity to characterize the mechanical properties of CMC samples.[12,17,18] In this study, a modified push-out testing method comprising unloading–reloading cycles for a quantitative evaluation of the interfacial fracture toughness is presented.

2. Experimental

2.1. Material and sample preparation

The specimen investigated in this study consists of SiC fiber (Tyranno Grade S, UBE Industries, Ltd.)-reinforced SiC matrix composites and are provided by MT Aerospace AG. Two-dimensional plain-woven SiC fiber fabrics were coated with a PyC layer by chemical vapor infiltration (CVI) method, and subsequently infiltrated via CVI process to form the SiC matrix. The samples have to be thinned precautiously to a final thickness typically below 100 μm. For that purpose, a slice of about 9 mm × 2 mm × 0.5 mm was cut by a precision low speed diamond saw (Isomet, Buehler) and thinned by a lapping process (Precision Lapping and Polishing System PM5, Logitech Ltd.) to generate plane-parallel sample surfaces perpendicular to the fiber orientation. During this procedure, the sample experienced minimal damage. The lapping suspension consisted of boron carbide particles with a grain size of 9 μm. Material of a minimum thickness of 200 μm was removed from each side of the sample. Final surface preparation consisted of polishing the specimen with a colloidal silica sol (mean particle size 32 nm) on both sides. The specimen then was placed on a glass substrate with a groove of 60 μm in width, and fixed by quartz wax ensuring close contact to the substrate. All the push-out measurements discussed in this study were carried out on the same sample with a thickness of 94 μm. In addition, some push-in tests were performed on a thicker sample of 400 μm to conclude whether there is an influence of the flexural stiffness on the shape of the load–displacement curve.

2.2. Single-fiber push-out test

Single-fiber push-out tests were performed using an Universal Nanomechanical Tester system (Asmec GmbH), which enables both load- and displacement-controlled experiments in normal direction with a resolution of 0.01 mN and 1 nm, respectively. The indenter tip is exchangeable and can be positioned with a lateral accuracy of about 1 μm. In this study, push-out experiments were carried out with diamond indenter tips of two different geometries: a Berkovich tip (three-sided pyramid with a total included angle of 142.3°) and a custom-made flat-end indenter tip (truncated four-sided pyramid with an edge length of 4.0 μm and a total included angle of 38.3°, Micro Star Technologies). The maximum indenter displacement without touching the matrix depends on the tip geometry and the fiber radius. In order to estimate the maximum indenter displacement, we assume the indenter tip is positioned centered on the fiber, the surrounding matrix does not deform and the fiber radius is varying between 4.0 μm and 5.0 μm. Then the maximum allowed indenter displacement is between 0.9 μm and 1.2 μm for the Berkovich tip and between 3.4 μm and 6.3 μm for the flat-end tip.

Fibers surrounded by various numbers of neighbouring fibers were selected randomly for push-out to represent fiber–matrix interaction in domains of different local fiber volume contents.

The push-out tests were performed under displacement-controlled mode to enable the measurement of load drops. Two different experimental procedures were used, a standard loading schedule and a schedule with several unloading–reloading cycles. In case of standard push-out experiments, a final displacement of 5000 nm was chosen with a displacement rate of 20 nm/s, in case of experiments with unloading–reloading cycles the displacement rate was set to 50 nm/s with unloadings at 500 nm, 1000 nm, 1500 nm, 2000 nm, 2500 nm and at 6000 nm. Each unloading segment was performed at 100 nm/s. In addition, a series of load–displacement measurements was stopped at different stages during loading for a microscopic analysis of the push-out progress. Those samples were unloaded, removed from the substrate and examined by Scanning Electron Microscopy (SEM) and Atomic Force Microscopy (AFM) on both front and back side.

2.3. Scanning Electron Microscopy and Atomic Force Microscopy

The sample surfaces were investigated by means of Field Emission Scanning Electron Microscopy (DSM 982 Gemini, Zeiss) with respect to accurate position of indent, contact area and damage on fiber, PyC coating and matrix after unloading. Atomic Force Microscopy (Dimension Icon, Bruker) was done to check the residual depth of indentation imprint and the extent

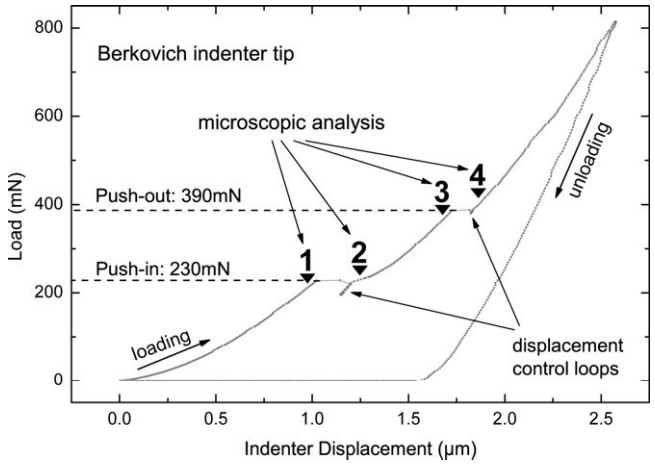

Fig. 1. Representative load–displacement diagram of a single-fiber push-out test performed with a Berkovich indenter tip. The stages at which measurements were stopped for microscopic analysis are indicated by arrows (1–4).

of residual displacement of fiber on front and back side after the experiment.

3. Results and discussion

3.1. Single-fiber push-out tests with Berkovich indenter tip

A typical load–displacement curve of a single-fiber push-out test performed with a diamond indenter tip of Berkovich geometry is shown in Fig. 1. Initial indenter displacement leads to an increase in load which is followed by a plateau-like behavior at 230 mN, a second increase in load until another plateau is reached at 390 mN, and a final rise until peak load. The retraction of the indenter tip then results in a decrease in load, reaching zero load at a displacement of 1.53 μm. The shape of the curve corresponds to Berkovich push-out curves described in literature,[4–6] except for the fact that in the measurements of the present study, the first plateau is considerably more pronounced.

For a detailed microscopic analysis of the progression of failure during push-out testing procedure, push-out measurements were stopped and unloaded at several different stages, four of which are marked in Fig. 1.

When interrupting the experiment at the end of the first rise in the load–displacement curve (Fig. 1, point 1), SEM micrographs of the front side of the sample (Fig. 2(a)) show a centered imprint of the pyramidal indenter tip on the fiber. The imprint is confined to the fiber cross-sectional area so that contact between indenter tip and the adjacent SiC matrix can be excluded. The depth of pyramidal imprint determined by AFM measurements amounts to 150 nm. There is no residual push-in of the fiber relative to the surrounding sample surface. On the back side of the sample, no indication of a push-out is found by AFM and SEM investigations. In addition to the pyramidal deformation of the fiber detected, elastic deformation must have occurred during the initial indenter displacement, as the indenter displacement of 1.0 μm (Fig. 1) exceeds the depth of imprint (150 nm) by far. As the fiber is mechanically coupled to the surrounding matrix via PyC interphase, elastic deformation takes place on both fiber and matrix. The upward curvature of the load–displacement curve is due to the pyramidal shape of the tip, i.e., due to the increase of the projected contact area between indenter tip and sample during loading.[19]

By increasing the load, stress at the fiber–matrix interface rises. When the local stress at the interface exceeds a critical value, an initial debonding crack is formed. In most of the experiments using a Berkovich tip, the crack initiation can not be assigned to a certain point in the load–displacement graph. The crack initiation causes partial debonding and mechanical decoupling of fiber and matrix. Consequently, there is a sudden decrease of elastic modulus of the fiber–matrix system which leads to an imbalance of forces and therefore to an abrupt displacement of the indenter tip. In the load–displacement curve, this results in a plateau-like behavior (between points 1 and 2 in Fig. 1, at 230 mN). The displacement control is not able to prevent this rapid movement, but subsequently retracts the tip which leads to a loop marked in Fig. 1. SEM micrographs of samples from push-out tests that were interrupted during the first plateau confirm that the indenter tip has solely contacted the fiber but not the surrounding matrix area.

In case the push-out test was interrupted right after the first plateau (Fig. 1, point 2), SEM analysis reveals plastic deformation on the fiber and on the adjacent matrix (marked in Fig. 2(b)) resulting from the Berkovich indenter tip. This finding proves that starting from the first plateau, both fiber and matrix are loaded directly by the indenter tip. On the back side of the sample, no deviations from the original state are observed by SEM (Fig. 2(c)) and AFM.

Further displacement of the indenter tip leads to another increase of load in the load–displacement diagram (Fig. 1, points 2 and 3), which is caused by increasing plastic and elastic deformations of fiber and matrix (Fig. 2(d)). Push-out tests that are interrupted and unloaded at the end of this regime (Fig. 1, point 3) show that the fiber surface was pushed-in a distance of 25 nm, in addition to the pyramidal imprint of 170 nm in depth, as detected from the AFM measurements (AFM image Fig. 3(a) and AFM cross section diagram Fig. 3(c)). On the back side of the sample, no indication of a push-out is found by SEM and AFM measurements.

The displacements of the fiber surface are illustrated in the schematic of Fig. 4. During loading, the fiber is pushed-in due to plastic and elastic deformations of fiber and surrounding matrix (dashed line). This corresponds to the indenter displacement shown in the load–displacement diagram (Fig. 1, point 3: 1680 nm). In this state of displacement, the crack has already propagated along the interface, but has not yet reached the back side of the sample (Fig. 4, zigzag line). After unloading of the sample, the elastic deformations relax and the residual push-in depth (Fig. 3(c), 25 nm) and the depth of the imprint (Fig. 3(c), 170 nm) are measured by AFM. These measurements imply an elastic deformation of 1485 nm under load.

Push-out tests that are aborted at this stage (Fig. 1, point 3) correspond to so-called push-in tests, which are usually performed on thick samples and are described in literature.[3,18,13,20–22]

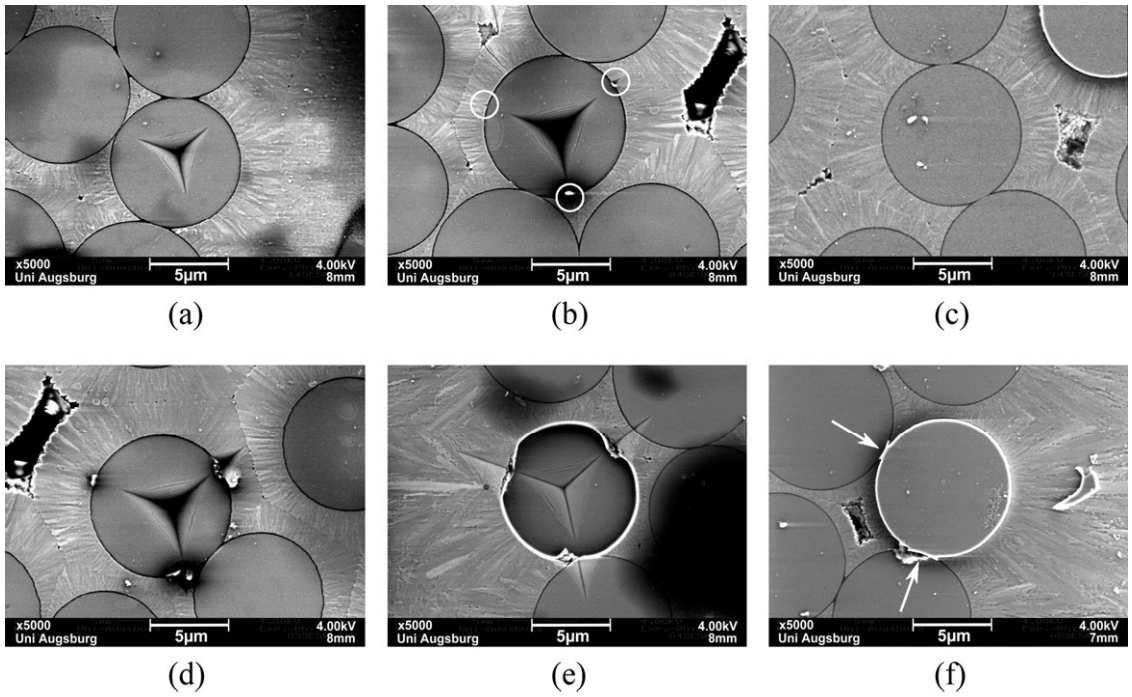

Fig. 2. SEM analysis of sample surfaces after interruption at different stages during single-fiber push-out tests performed with Berkovich indenter. The numbering of the stages refers to Fig. 1. (a) SEM micrograph of sample front side, loading stopped at point 1. The imprint of the Berkovich indenter tip is limited to the fiber cross section. (b) SEM micrograph of sample front side, loading stopped at point 2. The traces of contact between pyramidal indenter tip and matrix are marked. (c) SEM micrograph of sample back side, loading stopped at point 2. No deviations from the initial state are found. (d) SEM micrograph of sample front side, loading stopped at point 3. Plastic deformations of fiber and adjacent matrix are clearly visible. (e) SEM micrograph of sample front side, loading stopped at point 4. The dark color of the fiber indicates the push-out. Except for the pyramidal imprint, no further damage on fiber is observed. (f) SEM micrograph of sample back side, loading stopped at point 4. The fiber protrudes from the surface (push-out). The fact that the coating is pushed together with the fiber is specially evident (marked by arrows).

When the crack reaches the back side, fiber and matrix are completely debonded and the compressed fiber may expand to the back side towards the groove. The elimination of the fiber–matrix bonding together with a partial relaxation of the fiber leads to an imbalance of forces and therefore to a sudden displacement of the indenter tip, which causes the second plateau in the load–displacement diagram, at 390 mN (Fig. 1, between points 3 and 4).

Experiments that were stopped right after the second plateau (Fig. 1, point 4) reveal that the fiber is pushed-in a distance of about 790 nm with a pyramidal imprint of 260 nm (AFM image Fig. 3(b) and AFM cross section diagram Fig. 3(c)). Except for the pyramidal imprint, no further damage on the fiber is observed (Fig. 2(e)). On the back side of the sample, the fiber protrudes clearly from the surface (Fig. 2(f)) giving proof to the fact that a push-out takes place at the second plateau in the load–displacement diagram.

This process is illustrated in Fig. 5. The schematic points out that the indenter displacement (Fig. 1, point 4: 1870 nm) is equal to the sum of push-in depth (Fig. 3(c), 790 nm), the depth of the imprint (Fig. 3(c), 260 nm) and the elastic deformations of fiber and matrix (calculated 820 nm). The comparison of the 190 nm indenter displacement between point 3 and point 4 and the increase in plastic deformations (push-in depth and depth of imprint) of 855 nm seems to be in contradiction. This mismatch is explained by the relaxation of the compressed fiber: Before the crack reaches the back side of the sample (point 3), the fiber decompresses elastically towards the front side of the sample during unloading. After the crack has reached the back side of the sample, the fiber is debonded along the whole interface (point 4). At the moment push-out is initiated the fiber decompresses partially towards the back side, while contact to the indenter on the front side is still retained.

Debonding turns out to occur between PyC coating and matrix. The fact that the coating is pushed together with the fiber is specially evident at locations where the coating of the protruding fiber touches the one of a neighbouring fiber (marked in Fig. 2(f)).

After this plateau, another increase of load occurs (Fig. 1, point 4 up to peak load) with a slope similar to the slope between points 2 and 3. Experiments confirm that the push-out depth as well as the imprint on matrix grow when the loading is continued.

Complete unloading of the sample results in relaxation of the elastic deformation predominantly due to the matrix, reaching zero load at 1.53 µm (Fig. 1). This is in agreement with AFM measurements on the front side of the sample that show a residual fiber displacement of 1.5 µm relative to the sample surface.

In summary, load–displacement curves of single-fiber push-out tests carried out with a Berkovich indenter tip showed two pronounced plateaus: The first one can be attributed to the fiber push-in and the second one to the fiber push-out. It was found that the pyramidal indenter tip contacts the matrix starting at

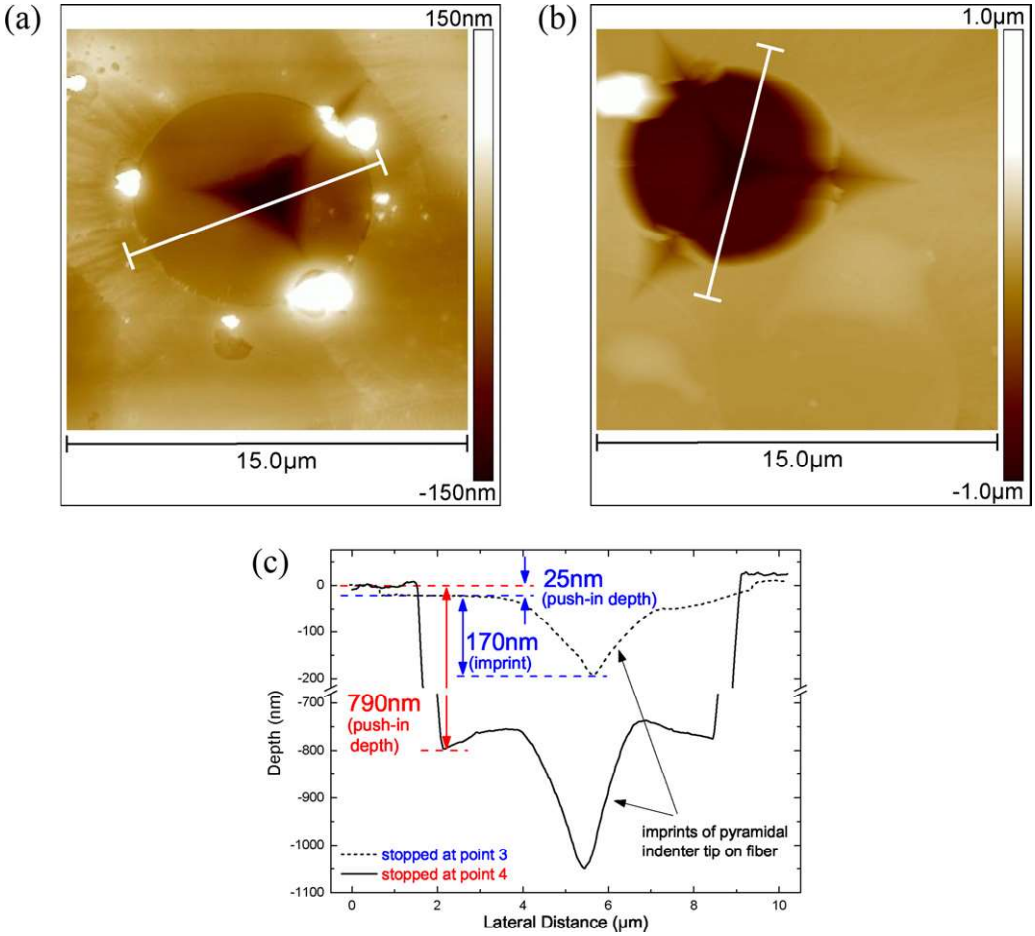

Fig. 3. AFM analysis of sample surfaces after interruption at different stages during single-fiber push-out tests performed with Berkovich indenter. The numbering of the stages refers to Fig. 1. (a) AFM image of sample front side, loading stopped at point 3. The section line marked corresponds to the profile diagram (Fig. 3(c)). (b) AFM image of sample front side, loading stopped at point 4. The section line marked corresponds to the profile diagram (Fig. 3(c)). (c) Profile sections from AFM measurements of sample front side. Loading was stopped at point 3 and point 4, respectively.

push-in. Accordingly, during crack propagation and push-out not only the fiber but also the surrounding matrix is directly loaded by the pyramidal indenter tip. This causes an overestimation of fiber–matrix interaction and, therefore, the test should be invalidated. In literature, contact between indenter tip and matrix is assumed not to occur before push-out,[4,5] although there is no proof whether this is the case. However, for a valid evaluation of the interfacial shear strength τ_{is} (Eq. (1)), it is necessary to verify that the tip contacts the fiber only.

3.2. *Single-fiber push-out tests with flat-end indenter tip*

Due to the fact that contact was observed between the Berkovich indenter tip and the SiC matrix before push-out, the single-fiber push-out tests and microscopic analyses were repeated using a flat-end indenter tip with a total included angle significantly smaller than in Berkovich geometry (see Section 2.2).

3.2.1. *Push-out tests with standard loading schedule*

In Fig. 6, the load–displacement curve of a flat-end indenter push-out test is shown in comparison to the Berkovich indenter experiment discussed in Section 3.1 (Fig. 1). The shape of the flat-end indenter curve is comparable to those known from literature, using a flat-end indenter.[12,16,10]

At the beginning of the experiment, the contact area between tip and fiber is formed. In the load–displacement curve (Fig. 6), this results in an increasing slope throughout the first 100 nm. The slope of the following part of the curve (Fig. 6, up to point A) is steeper and shows a smaller curvature than in the Berkovich

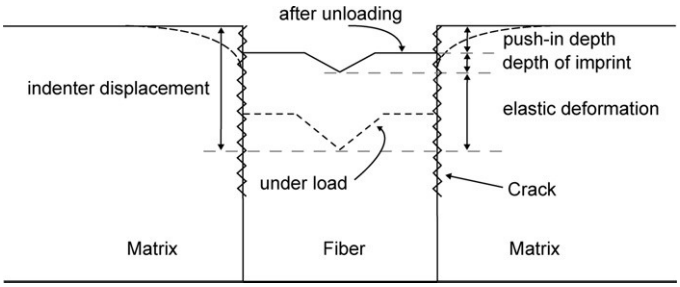

Fig. 4. Schematic illustration of plastic and elastic deformations of push-out sample at point 3 (point C, respectively). The dashed line marks the position of the fiber surface under load, the solid line shows it after unloading.

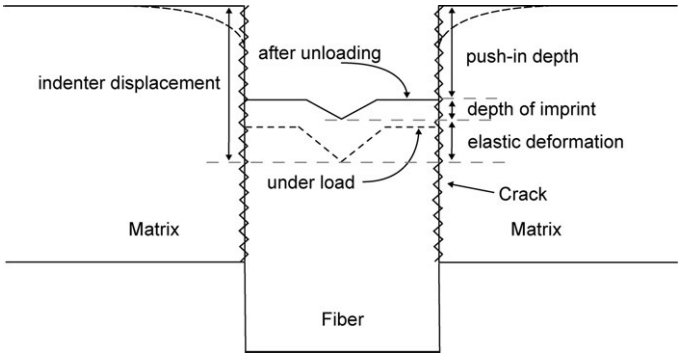

Fig. 5. Schematic illustration of plastic and elastic deformations of push-out sample at point 4 (point D, respectively). The dashed line marks the position of the fiber surface under load, the solid line shows it after unloading.

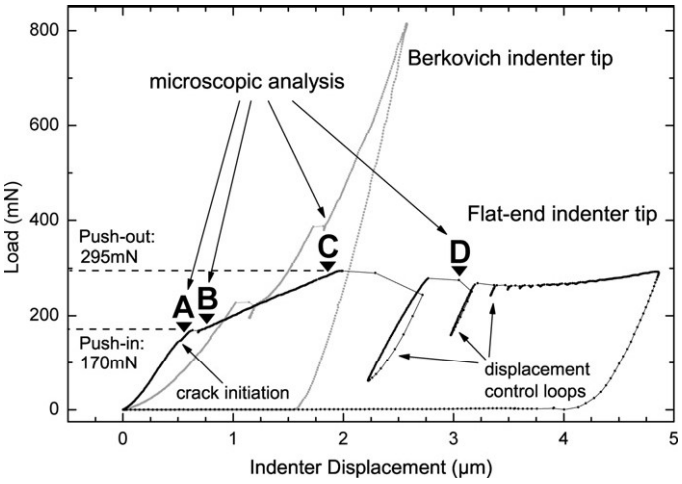

Fig. 6. Representative load–displacement diagram of a single-fiber push-out test performed with a flat-end indenter tip (black). The stages at which measurements were stopped for microscopic analysis are indicated with arrows (A–D). Load–displacement curve from push-out test with Berkovich indenter tip on same sample (Fig. 1) is added for comparison (gray).

case. In analogy to the Berkovich case, plastic deformation of fiber together with elastic deformation of fiber and matrix occurs in this part of the experiment. The steeper slope and the smaller curvature are attributed to the geometry of the tip. At 145 mN, there is a change in gradient (marked in Fig. 6), which is ascribed to crack initiation between fiber and matrix. This feature was found to appear at the same load in push-in tests for a much thicker sample of 400 µm thickness. This confirms that crack initiation is caused by a local stress field at the sample surface and therefore is independent of sample thickness.[12] Microscopic analyses of samples from push-out tests interrupted at point A show a centered imprint of the flat-end indenter tip on fiber (Fig. 7(a)) of 75 nm in depth. The expected debonding crack is not detectable by electron microscopy.

As soon as the crack encloses the fiber in the surface region, fiber and matrix are partially decoupled, which leads to an

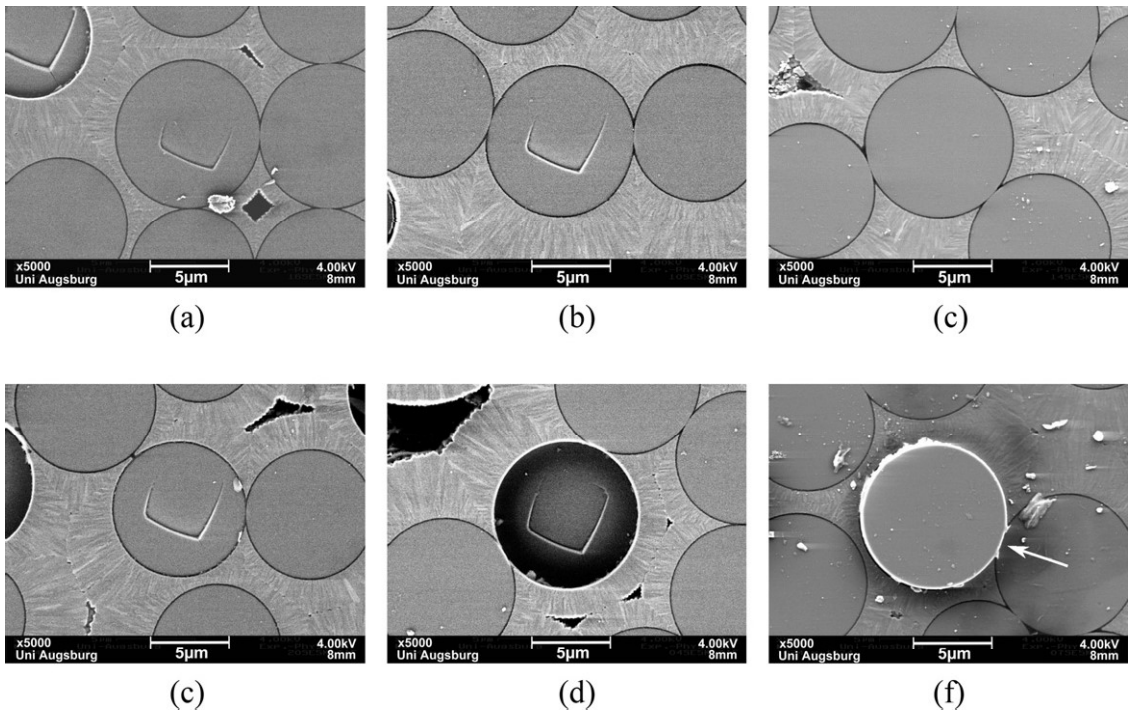

Fig. 7. SEM analysis of sample surfaces after interruption at different stages during single-fiber push-out tests performed with flat-end indenter. The numbering of the stages refers to Fig. 6. (a) SEM micrograph of sample front side, loading stopped at point A. Parts of the imprint of the flat-end indenter (truncated four-sided pyramid) are visible. (b) SEM micrograph of sample front side, loading stopped at point B. The imprint of the flat-end indenter tip is limited to the fiber cross section. (c) SEM micrograph of sample back side, loading stopped at point B. No deviations from the initial state are found. (d) SEM micrograph of sample front side, loading stopped at point C. There is almost no increase in the depth of imprint on fiber compared to the test interrupted at point B (Fig. 7(b)). (e) SEM micrograph of sample front side, loading stopped at point D. The fiber is pushed-out. There is no trace of any damage on the adjacent matrix caused by the flat-end indenter tip. (f) SEM micrograph of sample back side, loading stopped at point D. The fiber protrudes from the surface (push-out). Parts of the adjacent PyC coating are pushed-out together with the fiber (marked) indicating that debonding occurs between coating and matrix.

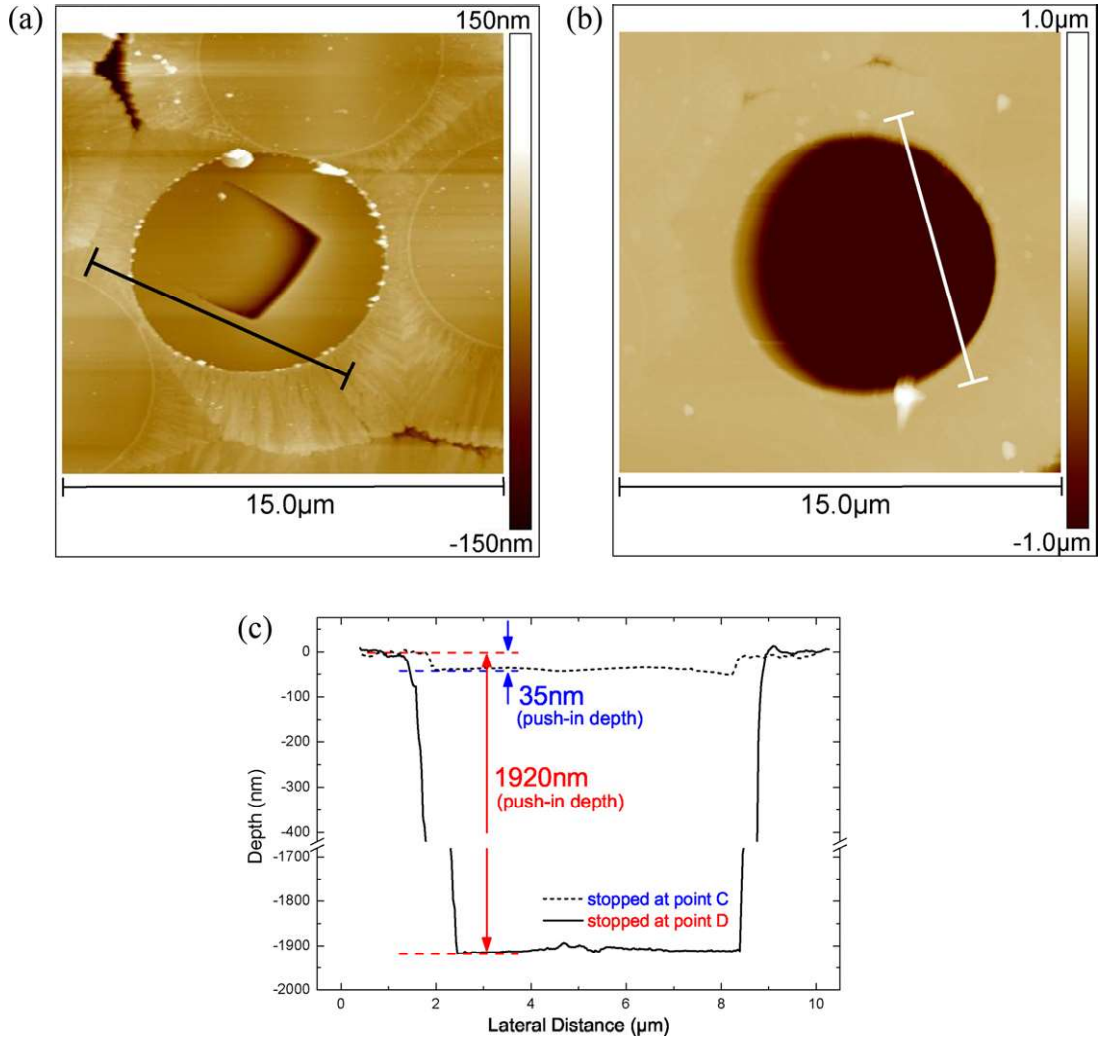

Fig. 8. AFM analysis of sample surfaces after interruption at different stages during single-fiber push-out tests performed with flat-end indenter. The numbering of the stages refers to Fig. 6. (a) AFM image of sample front side, loading stopped at point C. The section line marked corresponds to the profile diagram (Fig. 8(c)). (b) AFM image of sample front side, loading stopped at point D. The section line marked corresponds to the profile diagram (Fig. 8(c)). (c) Profile sections from AFM measurements of sample front side. Loading was stopped at point C and point D, respectively.

imbalance of forces and a first sudden crack growth. In the load–displacement curve, this behavior is reflected by a plateau at 170 mN (Fig. 6, between points A and B). SEM and AFM analyses of samples that have been unloaded right after the first plateau (Fig. 6, point B) confirm that there is no contact between the indenter tip and the matrix at this stage (Fig. 7(b)) and that there is a residual compression of the fiber of 20 nm after unloading. On the back side of the sample, no indication of a push-out is found by SEM (Fig. 7(c)) and AFM investigations.

After the first plateau, a long linear rise with a smaller slope than in the Berkovich case follows (Fig. 6, from point B to C). In contrast to the experiments using a Berkovich tip, SEM (Fig. 7(d)) and AFM analyses (Fig. 8(a)) of push-out tests that were interrupted at point C prove that there was no contact between tip and matrix during that stage, resulting in a more moderate slope. AFM and SEM measurements reveal that the depth of imprint (about 100 nm) stays almost constant between point B and point C (Fig. 7(b) and Fig. 7(d)). The residual push-in depth after unloading at point C amounts to 35 nm (Fig. 8(c)). Analysis of the reverse side of the sample demonstrates no deviations from the initial state. Loading experiments that are interrupted at the end of this linear regime correspond to the push-in testing procedure, usually performed on thick samples.[3,18,13,20–22] The dominating mechanisms in this regime are progressive, stable crack growth under shear loading as well as elastic deformation of fiber and matrix.

To illustrate the displacements at point C, we refer to the same schematic as for the Berkovich case (Fig. 4). Before the interfacial debonding (zigzag line) is complete, the fiber is solely pushed-in and not pushed-out on the sample back side. The indenter displacement at point C (1860 nm) is equal to the sum of the push-in depth (35 nm), the depth of imprint (100 nm) and the elastic deformation of fiber and matrix under load (calculated 1725 nm).

Since the surrounding matrix is not loaded directly by the tip, a lower force (295 mN) than in the Berkovich case (390 mN) is required to propagate the crack throughout the sample. Once debonding is completed (Fig. 6, beyond point C), elimination

of the fiber–matrix bonding and a partial relaxation of fiber compression lead to a sudden decrease in opposing forces. The imbalance of forces causes a rapid displacement of the indenter, resulting in displacement control loops (marked in Fig. 6). Interlocking between fiber and CVI-matrix as well as potentially existing residual radial thermal stresses prevent an abrupt drop of opposing forces and result in an average slow, continuous decrease in load over a distance of 1.6 μm. SEM micrographs (Fig. 7(e)) confirm that there is still no contact between the indenter tip and the matrix in this region (Fig. 6, point D). Micrographs of the back side surface (Fig. 7(e)) show the fiber protruding. The debonding takes place between PyC coating and matrix (as it does in Berkovich experiments). After unloading the sample at point D, AFM measurements on the sample front side reveal a residual push-in depth of about 1920 nm (AFM image Fig. 8(b) and AFM cross section diagram Fig. 8(c)) and a depth of imprint equal to that before push-out (100 nm).

As for the Berkovich case, Fig. 5 is used to schematically show the plastic and elastic deformations after push-out (point D). The indenter displacement of 3050 nm and residual deformations of 2020 nm (push-in and imprint) as measured by AFM result in a calculated elastic deformation of 1030 nm. Analogous to the Berkovich case, the mismatch between indenter displacement (point C to D) and push-in depth can be explained by a partial fiber relaxation towards the sample back side at the initiation of the push-out.

In the load–displacement diagram (Fig. 6), at an indenter displacement of about 3.6 μm, the force increases again, which is ascribed to an indenter-matrix contact. This is in good agreement with the geometrical calculation taking into account the geometry of the tip and the fiber diameter. Further displacement results predominantly in plastic and elastic deformation of the surrounding matrix. Total unloading causes a relaxation of elastic deformations and the load reaches zero at 4.0 μm (Fig. 6), which agrees to AFM measurements of the sample front side.

The load–displacement curves of push-in tests on a 400 μm thick sample do not show any systematic deviations from curves of the 94 μm thick sample up to point 3 (Fig. 1, Berkovich tip) and point C (Fig. 6, flat-end tip), respectively. This demonstrated that the flexural stiffness of the 94 μm thin sample does not affect the result of the measurement. Further indentation on thick samples did not cause push-out, but fiber cracking, so the loading was stopped.

In summary, using a custom-made flat-end indenter tip with a total included angle of 38.3°, the drawbacks of the Berkovich tip can be overcome. Microscopic analyses of samples after push-out tests confirm that in this case, no loading of the adjacent matrix takes place before push-out. The differences between the push-out curves of the two tip geometries considered can be explained consistently by the geometry of the respective tip. For the evaluation of the interfacial shear strength according to Marshall,[3] the load at push-out, i.e., the peak load in the flat-end indenter case, is normalized to the crack surface. The quantitative evaluation was performed based on a series of 32 push-out tests on the same sample of 94 μm thickness. The fibers varied from 7.4 μm to 10.4 μm in diameter and were spread across a sample area of several mm^2. The evaluation gives an interfacial shear strength of 105 MPa at a standard deviation of 11 MPa. We observed no difference resulting from different local fiber volume contents within the range of scatter.

In addition to the interfacial shear strength, the push-out curve allows the determination of the crack initiation force, although in most of our measurements this force is not distinguishable from the push-in plateau. In this cases, crack initiation was assumed to occur at the push-in plateau and the load at push-in was evaluated for crack initiation. An evaluation of 47 push-out tests leads to a crack initiation force of 186 ± 34 mN. But as the stress distribution at the surface is complex and strongly depends on microscopic defects of the interphase possibly introduced by surface preparation, the numerical value appears to be of limited significance for interpretation and evaluation of mechanical properties. On the other hand, the relatively small error might tell otherwise.

3.2.2. Push-out tests with unloading–reloading cycles for evaluation of interfacial fracture toughness

Most push-out studies focus on determining stress-based interfacial parameters, such as the interfacial shear strength and the stress for initial debonding.[3,13,9,7,16] As the precise stress distribution along the interface is unknown, these evaluation methods depend on assumptions concerning the stress distribution, including the effects from Poisson's expansion and from interfacial roughness.

Taking into account that debonding takes place by a dissipative propagation of a crack along the fiber, the interfacial fracture toughness can be considered as the most evident and preferable quantity to be determined. It characterizes the debonding behavior of a composite sample and is most relevant for the prediction of mechanical properties of macroscopic specimens.[12,18,17]

In the present study, a straightforward energy-based approach to extract the interfacial fracture toughness from single-fiber push-out test data is presented, which does not require assumptions regarding the stress distribution along the interface.

The interfacial fracture toughness is a material property which describes the ability of a sample to resist crack propagation. It can be defined by means of the strain energy release rate. The strain energy release rate G is the energy ∂U dissipated during fracture per unit of newly created fracture surface area ∂a

$$G = -\frac{\partial U}{\partial a} \tag{2}$$

In this study, the interfacial fracture toughness $\langle G \rangle$ of a sample is taken as the strain energy release rate G averaged over the area of stable crack growth A_{crack}

$$\langle G \rangle = -\frac{\Delta E_{\mathrm{crack}}}{A_{\mathrm{crack}}} \tag{3}$$

where $\Delta E_{\mathrm{crack}}$ designates the energy which is dissipated in the creation of the new surfaces arising from crack propagation.

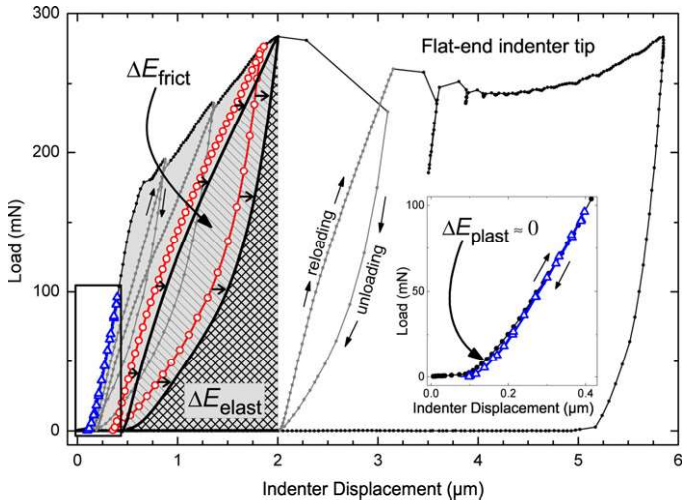

Fig. 9. Load–displacement diagram of modified single-fiber push-out test for evaluation of interfacial fracture toughness. Unloading–reloading cycles were added to the loading schedule to enable the separation of the elastic and plastic energy portions. Inset: Enlargement of the lower left part of the diagram.

The work done by the indenter up to peak load W_{ind} is equal to the sum of the dissipative energy contribution $\Delta E_{\text{dissipative}}$ and the non-dissipative energy contribution $\Delta E_{\text{non-dissipative}}$:

$$W_{\text{ind}} = \Delta E_{\text{dissipative}} + \Delta E_{\text{non-dissipative}} \tag{4}$$

The dissipative energy portion $\Delta E_{\text{dissipative}}$ comprises the crack energy ΔE_{crack}, the energy ΔE_{plast} for plastic deformation of the fiber and the work of friction ΔE_{frict} which is done during movement of the debonded part of the fiber relative to the matrix:

$$\Delta E_{\text{dissipative}} = \Delta E_{\text{crack}} + \Delta E_{\text{plast}} + \Delta E_{\text{frict}} \tag{5}$$

The work of friction ΔE_{frict} includes a component which results from the radial expansion of the fiber due to Poisson's effect.

The non-dissipative energy portion $\Delta E_{\text{non-dissipative}}$ is equal to the elastic deformation energy of fiber and matrix ΔE_{elast}:

$$\Delta E_{\text{non-dissipative}} = \Delta E_{\text{elast}} \tag{6}$$

Combined with Eqs. (4) and (5), this leads to:

$$\Delta E_{\text{crack}} = W_{\text{ind}} - \Delta E_{\text{plast}} - \Delta E_{\text{elast}} - \Delta E_{\text{frict}} \tag{7}$$

In order to determine the crack energy ΔE_{crack} during crack propagation and accordingly the interfacial fracture toughness $\langle G \rangle$ of the sample, the loading schedule of the push-out test has been modified. In a series of push-out tests performed with the flat-end indenter tip, unloading–reloading cycles were added to the standard loading schedule. The concise parameters of the modified schedule are given in Section 2.2. By comparing the modified measurement (Fig. 9) with the standard measurement (Fig. 6), it can be seen that the standard load–displacement curve forms the envelope to the curve of the modified test.

The work done by the indenter W_{ind} can be determined by integration of the load–displacement curve from zero to its maximum value (Fig. 9, gray-shaded area).

Microscopic analysis showed that plastic deformation exclusively occurs on the fiber and predominately takes place in the initial part of the load–displacement curve (Section 3.2.1). Thus, the energy dissipated in plastic deformation ΔE_{plast} can be assessed by means of an unloading–reloading cycle during the first rise in the load–displacement diagram (Fig. 9, inset, blue open triangles). The energy portion ΔE_{plast} corresponds to the area between the first loading and unloading curve (Fig. 9, inset) and is negligible compared to the other areas involved in this consideration.

For an accurate determination of the elastic energy ΔE_{elast} deposited in the sample and the friction energy ΔE_{frict} up to push-out, an unloading–reloading cycle exactly at peak position would be needed. Although this is technically not accessible, ΔE_{elast} and ΔE_{frict} can be quantified by the following approximation: The unloading and reloading curves of the cycle preceding the actual push-out (Fig. 9, red open circles) are shifted parallel, and their peak value is extrapolated to the actual peak load (Fig. 9, black solid lines). Integration of the shifted unloading curve yields ΔE_{elast} (Fig. 9, cross-hatched area) and integration of the area enclosed by the shifted unloading–reloading cycle gives ΔE_{frict} (Fig. 9, hatched by parallel lines). Following this procedure, ΔE_{crack} can be calculated from Eq. (7).

For the evaluation of the true interfacial fracture toughness $\langle G \rangle$, a separation of different dissipative and non-dissipative energy contributions during push-out experiments is required. In literature,[7,23] the fiber-end displacement is derived from the measured indenter displacement by subtracting an empirical calibration curve. The calibration curve is assumed to describe the elastic deformation of fibers and the penetration of the indenter tip, and is obtained by an indentation of fibers perpendicular to the fiber axis. In the present study, no such calibration curve is needed, as unloading–reloading cycles performed during the push-out measurements are used to separate the dissipative and non-dissipative energy contributions from each other. This enables the direct determination of the elastic energy of the individually tested fiber and surrounding matrix, and the dissipated energy at once.

In this study, stable crack growth along the complete debonding length is presumed, even though unstable crack propagation might occur at the end of the debonding process.[12] Accordingly, the area of stable crack growth A_{crack} is equated to the cylindrical surface of the tested fiber.

From the values for ΔE_{crack} and A_{crack}, the interfacial fracture toughness $\langle G \rangle$ can be determined (Eq. (3)). An evaluation of 30 push-out tests performed on fibers spread across a sample area of several mm^2 results in an interfacial fracture toughness of 44 J/m^2 at a standard deviation of 9 J/m^2. The numerical value is considered to be of plausible magnitude, since interfacial fracture toughness values as high as 28 J/m^2 have already been predicted to be compatible with acceptable mechanical behavior in SiC/PyC/SiC ceramic matrix composites.[15]

The application of the modified push-out testing procedure overcomes some drawbacks of the standard push-out method. The evaluation of the standard push-out test is based on a simple force balance and is used to determine the respective shear stress, at which the fiber debonding is completed and the push-out is initiated. The process of debonding, i.e., the

crack propagation along the interface is not taken into account.[12] In addition, in the standard approach all kind of dissipative effects are neglected to evaluate the interfacial shear strength τ_{is}, although frictional effects and Poisson's expansion are known to have a significant influence on push-out behavior.[24] Accordingly, the quantity determined in the standard approach can be interpreted as an upper limit for the critical shear stress. There are various approaches to include the dissipative effects in the evaluation, but these require additional assumptions concerning the stress field at the interface. With the modified push-out test presented in this study, no assumptions are required for the stress distribution and the frictional quantities, as the dissipative and non-dissipative energy contributions are measured directly. Moreover, the interfacial fracture toughness $\langle G \rangle$ determined here is the relevant quantity for the prediction of mechanical properties of macroscopic specimens, since it characterizes the crack growth, which actually leads to the interface failure.[12,18,17] However, as the additional unloading–reloading cycles do not affect the load for push-out initiation, both the evaluation of the interfacial shear stress and the evaluation of the interfacial fracture toughness $\langle G \rangle$ can be performed based on the same measurement.

4. Conclusions

A detailed microscopic analysis of single-fiber push-out tests on fiber-reinforced SiC/PyC/SiC composites has been carried out to investigate the progression of failure during testing procedure. For this purpose, push-out experiments performed with a Berkovich and a flat-end indenter tip have been stopped at different stages during loading schedule. The front and back sides of the samples were investigated at these different stages utilizing SEM and AFM measurements. Based on the microscopic observations, the load–displacement curves were discussed and the deviations in the load–displacement diagrams of the Berkovich and the flat-end indenter could be explained.

In particular, the microscopic analysis has revealed that the Berkovich indenter tip contacts the matrix adjacent to the fiber before push-out takes place and therefore leads to an overestimation of the interfacial parameters to be determined. The premature loading of adjacent matrix can be prevented by using a flat-end indenter tip with a suitable geometry.

In addition to the microscopic analysis of push-out tests with a standard loading schedule, an energy-based approach to determine the interfacial fracture toughness was applied to a load–displacement curve from a modified loading schedule comprising unloading–reloading cycles. Following this method, the interfacial fracture toughness can be quantified from a load–displacement curve without assumptions about the stress distribution along the interface. The interfacial fracture toughness is considered to be a significant quantity to assess the fiber–matrix debonding behavior in CMC. For the SiC/PyC/SiC sample investigated, it amounts to $44 \pm 9\,\mathrm{J/m^2}$, presuming no unstable crack propagation.

In future studies, the assumption of stable crack growth along the complete debonding length should be investigated, and the interfacial fracture toughness determined by modified push-out tests shall be correlated with fracture mechanical quantities obtained from macroscopic testing procedures.

Acknowledgements

The authors would like to thank MT Aerospace AG, especially Dr. K. Handrick, for kindly providing the CMC sample and for fruitful discussion.

References

1. Naslain R. The design of the fibre–matrix interfacial zone in ceramic matrix composites. *Composites Part A* 1998;**29**:1145–55.
2. Evans A, Zok F. The physics and mechanics of fiber-reinforced brittle-matrix composites. *J Mater Sci* 1994;**29**:3857–96.
3. Marshall D. An indentation method for measuring matrix-fiber frictional stresses in ceramic composites. *J Am Ceram Soc* 1984;**67**:C259–60.
4. Hinoki T, Zhang W, Kohyama A, Sato S, Noda T. Effect of fiber coating on interfacial shear strength of SiC/SiC by nano-indentation technique. *J Nucl Mater* 1998;**258**:1567–71.
5. Yang W, Kohyama A, Noda T, Katoh Y, Hinoki T, Araki H, Yu J. Interfacial characterization of CVI-SiC/SiC composites. *J Nucl Mater* 2002;**307**:1088–92.
6. Hinoki T, Yang W, Nozawa T, Shibayama T, Katoh Y, Kohyama A. Improvement of mechanical properties of SiC/SiC composites by various surface treatments of fibers. *J Nucl Mater* 2001;**289**:23–9.
7. Rebillat F, Lamon J, Naslain R, Lara-Curzio E, Ferber M, Besmann T. Interfacial bond strength in SiC/C/SiC composite materials, as studied by single-fiber push-out tests. *J Am Ceram Soc* 1998;**81**:965–78.
8. Rebillat F, Lamon J, Guette A. The concept of a strong interface applied to SiC/SiC composites with a BN interphase. *Acta Mater* 2000;**48**:4609–18.
9. Lara-Curzio E, Ferber M. Methodology for the determination of the interfacial properties of brittle-matrix composites. *J Mater Sci* 1994;**29**:6152–8.
10. Chandra N, Ghonem H. Interfacial mechanics of push-out tests: theory and experiments. *Composites Part A* 2001;**32**:575–84.
11. Watanabe K, Kohyama A, Sato S, Serizawa H, Tsunakawa H, Hamada K, Kishi T. Evaluation of interfacial shear strength of C/C composites by means of micro-indentation test. *Mater Trans JIM* 1996;**37**:1161–5.
12. Kerans R, Parthasarathy T. Theoretical analysis of the fiber pullout and pushout tests. *J Am Ceram Soc* 1991;**74**:1585–96.
13. Hsueh C. Evaluation of interfacial properties of fiber-reinforced ceramic composites using a mechanical-properties microprobe. *J Am Ceram Soc* 1993;**76**:3041–50.
14. Hsueh C, Rebillat F, Lamon J, Lara-Curzio E. Analyses of fiber push-out tests performed on Nicalon/SiC composites with tailored interfaces. *Compos Eng* 1995;**5**:1387–401.
15. Kerans R, Parthasarathy T, Rebillat F, Lamon J. Interface properties in high-strength Nicalon/C/SiC composites, as determined by rough surface analysis of fiber push-out tests. *J Am Ceram Soc* 1998;**81**:1881–7.
16. Rebillat F, Lamon J, Naslain R, Lara-Curzio E, Ferber M, Theodore M. Properties of multilayered interphases in SiC/SiC chemical-vapor-infiltrated composites with "weak" and "strong" interfaces. *J Am Ceram Soc* 1998;**81**:2315–26.
17. He M-Y, Hutchinson JW. Kinking of a Crack Out of an Interface. *J Appl Mech* 1989;**56**:270–8.
18. Marshall D, Oliver W. Measurement of interfacial mechanical-properties in fiber-reinforced ceramic composites. *J Am Ceram Soc* 1987;**70**:542–8.
19. Oliver W, Pharr G. An improved technique for determining hardness and elastic-modulus using load and displacement sensing indentation experiments. *J Mater Res* 1992;**7**:1564–83.
20. Kerans R, Rebillat F, Lamon J. Fiber–matrix interface properties of single-fiber microcomposites as measured by fiber pushin tests. *J Am Ceram Soc* 1997;**80**:506–8.

21. Kalinka G, Leistner A, Hampe A. Characterisation of the fibre/matrix interface in reinforced polymers by the push-in technique. *Compos Sci Technol* 1997;**57**:845–51.
22. Kuntz M, Grathwohl G. Advanced evaluation of push-in data for the assessment of fiber reinforced ceramic matrix composites. *Adv Eng Mater* 2001;**3**:371–9.
23. Rebillat F, Lamon J, Naslain R. Multilayered Interphases in SiC/SiC Composites: Influences of the Interfacial Bond Strength on the Interfacial Characteristics. *Key Eng Mater* 1999;**164-165**:361–4.
24. Parthasarathy TA, Barlage DR, Jero PD, Kerans RJ. Effect of interfacial roughness parameters on the fiber pushout behavior of a model composite. *J Am Ceram Soc* 1994;**77**:3232–6.